Physics Letters A 377 (2013) 2398–2402

Contents lists available at SciVerse ScienceDirect

Physics Letters A

www.elsevier.com/locate/pla

Electronic and optical properties of kesterite Cu_2ZnSnS_4 under in-plane biaxial strains: First-principles calculations

Chun-Ran Li [a,b], Yong-Feng Li [a,c,*], Bin Yao [a,c,*], Gang Yang [c], Zhan-Hui Ding [a], Rui Deng [d], Lei Liu [e]

[a] State Key Laboratory of Superhard Materials and College of Physics, Jilin University, Changchun 130012, China
[b] College of Mathematics and Physics, Bohai University, Jinzhou 121013, China
[c] Key Laboratory of Physics and Technology for Advanced Batteries (Ministry of Education), College of Physics, Jilin University, Changchun 130012, China
[d] School of Materials Science and Engineering, Changchun University of Science and Technology, Changchun 130022, China
[e] State Key Laboratory of Luminescence and Applications, Changchun Institute of Optics, Fine Mechanics and Physics, Chinese Academy of Sciences, No. 3888 Dongnanhu Road, Changchun 130033, China

ARTICLE INFO

Article history:
Received 22 April 2013
Received in revised form 28 June 2013
Accepted 28 June 2013
Available online 4 July 2013
Communicated by R. Wu

Keywords:
Cu_2ZnSnS_4
Biaxial strain
First-principle calculation
Electronic structure
Optical property

ABSTRACT

The electronic structures and optical properties of Cu_2ZnSnS_4 (CZTS) under in-plane biaxial strain were systematically investigated using first-principles calculations based on generalized gradient approximation and hybrid functional method, respectively. It is found that the fundamental bandgap at the Γ point decreases linearly with increasing tensile biaxial strain perpendicular to *c*-axis. However, a bandgap maximum occurs as the compressive biaxial strain is 1.5%. Further increase of compressive strain decreases the bandgap. In addition, the optical properties of CZTS under biaxial strain are also calculated, and the variation trend of optical bandgap with biaxial strain is consistent with the fundamental bandgap.

1. Introduction

The quaternary semiconductor, Cu_2ZnSnS_4 (CZTS), has attracted considerable attention for its potential applications in photovoltaic devices [1–3]. The CZTS is one of the promising absorption layer materials in thin film solar cells due to its suitable bandgap (∼ 1.5 eV) [4], high absorption coefficient (10^4 cm^{-1}) [5], containing earth-abundant elements and low costs [6]. Recent years, extensive researches on CZTS have been made experimentally and theoretically. Todorov et al. reported that they produced $Cu_2ZnSn(S,Se)_4$-based solar cell with a power conversion efficiency of 11.1% [7], which is a new efficient record so far. However, it still has a long way to reach the theoretical limit of more than 30% [8]. In order to further improve the device performance, it is crucial to understand more about the physical properties and underlying mechanism of CZTS material as a solar cell absorber layer.

Some effects induced by strain have been intensely investigated over the past ten years, such as GaN-based [9,10] and ZnO-based materials [11–13], revealing that the residual strains had definitely influence on electronic and optical properties. As a potential and promising thin-film solar cell material, the CZTS films are usually heteroepitaxially grown on glass substrates with Mo or CdS layers. It is inevitable that stress (or strain) appears in the films for heteroepitaxially growth process due to lattice mismatch and thermal expansion coefficient difference between the substrate and the film. It is known that the biaxial stress or strain generally plays an important role on crystal quality, physical properties and electronic structures of photoelectronic materials, especially based on thin film. In case of solar cell, the open circuit voltage, which is a key parameter to determine the energy conversion efficiency, is generally influenced by bandgap of thin film [14]. Therefore, it is significant to study the influence of biaxial strains on the electronic structure, crystal quality and device performance of the CZTS. However, up to now, experimental and theoretical studies of biaxial strains in CZTS have not been reported.

In this work, we carried out first-principles calculations on electronic structures and optical properties of CZTS under in-plane biaxial strains. Biaxial strain-dependent bandgap, splitting of crystal field energy, optical properties of CZTS are systematically investigated.

* Corresponding authors at: State Key Laboratory of Superhard Materials and College of Physics, Jilin University, Changchun 130012, China. Tel.: +86 431 85168857; fax: +86 431 85168857.
E-mail addresses: liyongfeng@jlu.edu.cn (Y.-F. Li), binyao@jlu.edu.cn (B. Yao).

0375-9601/$ – see front matter
http://dx.doi.org/10.1016/j.physleta.2013.06.046

2. Methods

The first-principles calculations in this work were performed with a plane-wave pseudopotential method. The crystalline structure of CZTS was optimized by the CASTEP code [15], in which the total energy is minimized from all atomic configurations. In the optimization process, we used generalized gradient approximation (GGA) in the scheme of Perdew–Burke–Eruzerhof (PBE) to describe the exchange and correlation functional. Vanderbilt-type ultrasoft pseudopotential [16], which allows calculations to be performed with the lowest possible cutoff energy for the plane-wave basis set, is used to describe the electron–ion interactions. It is well known that the fundamental bandgap in semiconductors and insulators is largely underestimated in GGA calculations, and this problem has been overcome by hybrid functional within the B3LYP scheme [17], in which the nonlocal Hartree–Fock approach is mixed into the energy functional of the GGA. This functional has been shown to reproduce observed bandgaps reliably in a wide variety of materials [18]. Thus in the electronic and optical properties calculations, we applied GGA as well as hybrid functional. The Cu $3d^{10}4s^1$, Zn $3d^{10}4s^2$, Sn $5s^25p^2$ and S $3s^23p^4$ with core electrons, were treated as valence electrons in the calculation. The valence electron wave functions were expanded in a plane-wave basis set up to a kinetic energy cutoff of 310 eV. This converges total energy differences to less than 1×10^{-6} eV/atom. For k-points sampling, a $3 \times 3 \times 1$ Monkhorst–Pack mesh in the Brillouin zone was used. In the hybrid calculation, norm-conserving pseudopotential was used, and the cutoff energy was set to 800 eV.

The structure of the kesterite CZTS (space group I-4) is quaternary with 16 atoms in conventional unit cell with two lattice constants a and c. The experimental lattice constants, $a = 0.5428$ nm and $c = 1.0864$ nm [19], were used to construct initial primitive cell for CZTS. The optimized structural parameters are $a = 0.5488$ nm and $c = 1.0953$ nm, with errors of $\sim 1\%$ with respect to experiment. The calculated lattice constants are also consistent with the ones calculated by others [20–22]. The definition of the strains paralleled to a- and c-axis can be found in Ref. [10]:

$$\varepsilon_{11} = \varepsilon_{22} = \frac{a - a_0}{a_0}, \tag{1a}$$

$$\varepsilon_{33} = \frac{c - c_0}{c_0}, \tag{1b}$$

where $a_0(a)$ and $c_0(c)$ denote the lattice constants of the unstrained (strained) crystal, and $\varepsilon_{11} < 0$ ($\varepsilon_{11} > 0$) represents layers under compressive (tensile) in-plane strain. In the limit of small deviations from the equilibrium, Hook's law can be expressed as the following matrix form:

$$(\sigma_{ij}) = (C_{ij})(\varepsilon_{ij}), \quad i, j, k = 1, 2, 3, \tag{2}$$

where σ_{ij}, ε_{ij} and C_{ij} are the elements of stress tensor, strain tensor, and elastic constants, respectively. Their main diagonal elements σ_{ij} and ε_{ij} ($i = j$) are the normal stress and strain. The nondiagonal elements σ_{ij} and ε_{ij} ($i \neq j$) can be zero by choosing appropriated coordinate frame. Only six of the nine elements C_{ij} are independent due to the symmetry of kesterite CZTS and they are C_{11}, C_{12}, C_{13}, C_{33}, C_{44} and C_{66}.

For an isotropic biaxial stress $\sigma_{11} = \sigma_{22}$ perpendicular to the c-axis, and the forces along the c-axis, $\sigma_{33} = 0$, the biaxial relaxation coefficient R^B is defined as $R^B = -\varepsilon_{33}/\varepsilon_{11}$. Moreover the relation between R^B and the stiffness constant C_{ij} is given by $R^B = 2C_{13}/C_{33}$ which means that the tensile biaxial strain in the ab plane results in compressive uniaxial strain along the c-axis [23]. In order to determine the biaxial relaxation coefficient R^B, we choose the lattice constant a close to the equilibrium one and, in each case, minimize the total energy of the system with respect to the second lattice constant c to obtain the relaxed value of c.

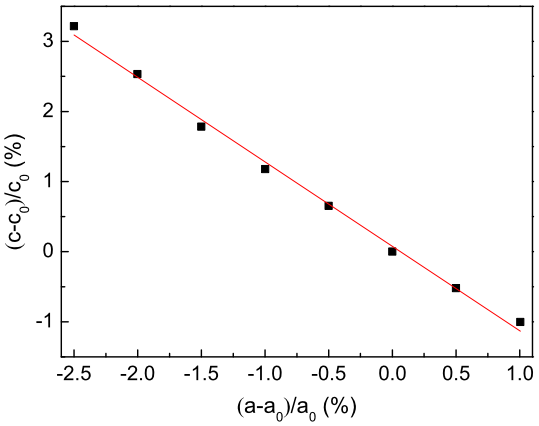

Fig. 1. The c-axis strain as a function of in-plane biaxial strain.

Table 1
Calculated elastic constant C_{ij}, bulk modulus B, Poisson ratio υ and Young modulus E. Except unitless Poisson ratio, all remaining elastic properties are in GPa.

C_{11}	C_{12}	C_{13}	C_{33}	C_{44}	C_{66}	B	υ	E
80.77	44.25	45.01	76.95	42.08	44.29	56.31	0.33	48.52

3. Results and discussion

3.1. Crystalline structure under biaxial strain and elastic constants

Fig. 1 shows the dependence of biaxial in-plane strain on c-axis strain of kesterite CZTS. As expected, the increases of in-plane tensile strain results in the decrease of the c-axis lattice constant due to Poisson effect. We obtained a slope of -1.23 by linearly fitting the data, suggesting $R^B = -\varepsilon_{33}/\varepsilon_{11} = 1.23$. For comparison, we also performed the calculations of elastic constants, as listed in Table 1. The elastic constant ratio of $2C_{13}/C_{33}$ is 1.17, which is in good accordance with the previous report [24] and close to $-\varepsilon_{33}/\varepsilon_{11} = 1.23$.

3.2. Electronic structures under biaxial strain

The calculated bandgap (E_g) versus biaxial strains are shown in Fig. 2. The unstrained bandgap calculated by PBE is 0.03 eV, which is consistent with the previous results from LDA [22] or GGA [25] calculations. This value will decrease lineally with the increase of tensile strains. When the tensile strain reaches $+1\%$, the fundamental gap is close to zero. We have to point that this value obviously deviates from the experimental results. As mentioned above, the deviation attributes to natural defects of PBE exchange correlation functional in calculating excitation states energies. Hybrid functional method such as B3LYP which is able to predict bandgaps in good agreement with experiment for a wide range of materials [18] is used to reproduce the bandgap. Calculations using B3LYP converge to results around 1.388 eV for the strain-free structure, which is comparable to the theoretical and experimental values [4,21,26]. Although PBE and B3LYP functional have obtained disparate results, the bandgaps show a similar variation tendency with various biaxial strains. The bandgap decreases linearly with the increase of tensile strain. However, it is noted that there exists a bandgap maximum as the compressive strain is -1.5%. The bandgap increases with the increase of compressive biaxial strain for $\varepsilon_{11} > -1.5\%$, but decreases for $\varepsilon_{11} < -1.5\%$.

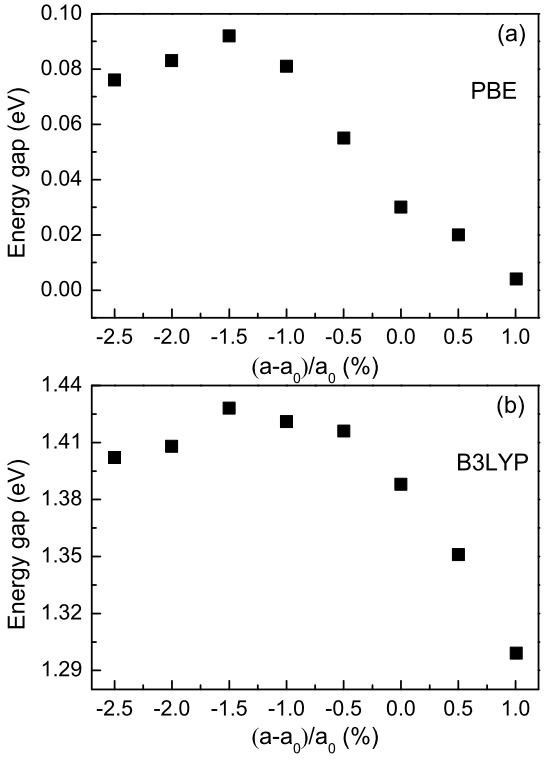

Fig. 2. The energy gap at Γ point of CZTS as the function of the in-plane biaxial strain from (a) PBE and (b) B3LYP results, respectively.

The band structures of kesterite CZTS are plotted at strains of +1% and −1.5% in Fig. 3. To illustrate the strain effect, the unstrained one (solid line) is also presented. Both the VBM and the CBM occur at the Γ point $k = 0$ indicating that CZTS is a direct bandgap semiconductor. It is observed that for the compressed CZTS, the increased overlap between the orbital in the biaxial plane led to an overall broadening of the conduction and valence bands. On the contrary, the tensile strains resulting in the narrowing between the conduction bands and valence bands. For both computational schemes, the band topology is very similar as far as the conduction band is concerned, since B3LYP essentially shifts the conduction bands to higher energies. Furthermore, the top of the VB is split by the crystal field and the spin–orbit interaction [4]. At the VBM the tetrahedral crystal field split-off $\Delta_{cf} > 0$ denotes as the case when the double degenerate VB is energetically higher than the single degenerate band. In our calculation, the split energy of unstrained CZTS is a small and negative value (−62 meV), in agreement with Persson (−33 meV) [4] and Chen et al. (−65 meV) [27]. As shown in Fig. 4, with the increasing of compressive strain, the crystal split energy increases from negative to positive at −1.5% strains, where the topmost of valence band is rearranged. The rearrangement of valence might cause the emergence of bandgap maximum. We note that our calculation has overestimated the Δ_{cf}, it might be because of the underestimate of the fundamental gap increases the repulsive coupling between the valence and conduction band states at Γ point. As spin–orbit coupling and spin degrees of freedom are neglected in our calculation, therefore we could not see the removal of the double degenerated states.

3.3. Optical properties under biaxial strain

The optical properties of matters can be described by means of the transverse dielectric function $\varepsilon(\omega) = \varepsilon_1(\omega) + i\varepsilon_2(\omega)$. The imaginary part $\varepsilon_2(\omega)$ could be calculated from the momentum matrix elements between the occupied and unoccupied wave functions within the selection rules, and the real part $\varepsilon_1(\omega)$ can be evaluated from imaginary part $\varepsilon_2(\omega)$ by Kramers–Kronig relationship. All the other optical constants, such as reflectivity $R(\omega)$, absorption

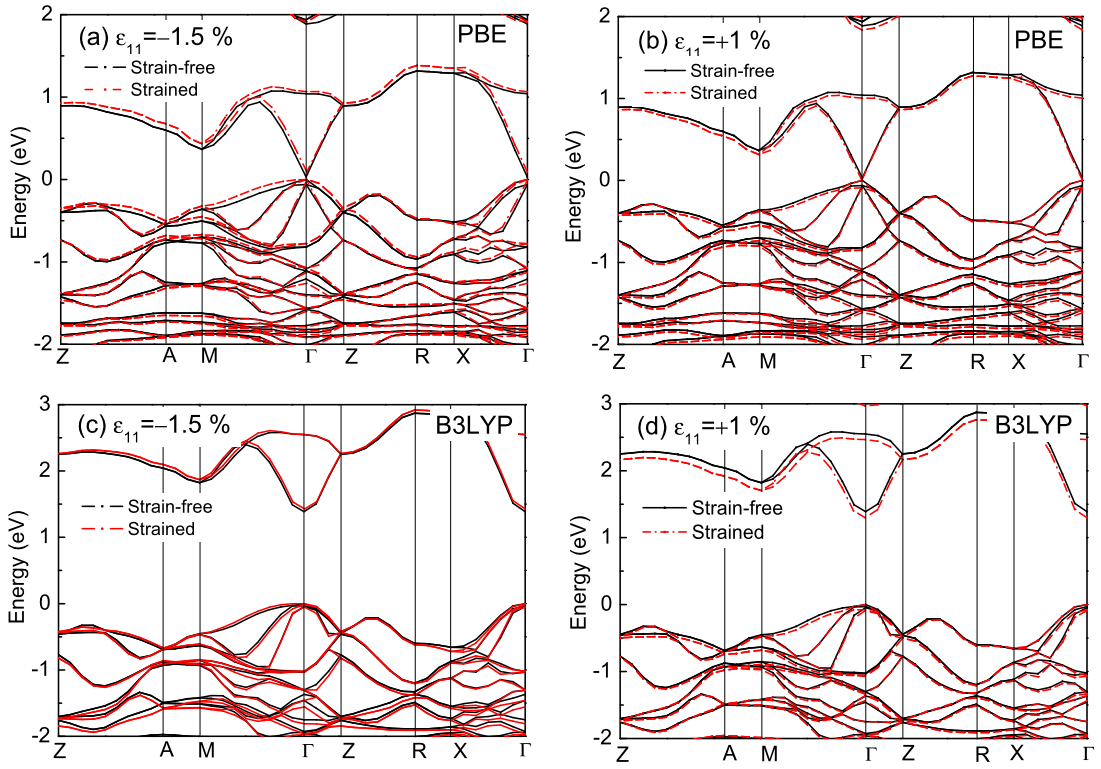

Fig. 3. Band structures of CZTS under biaxial strains of (a), (c) −1.5% and (b), (d) +1% with respect to the unstrained one. The solid lines in all figures present the unstrained results. (a) and (b) are calculated using PBE functional, whereas (c) and (d) are calculated using B3LYP functional.

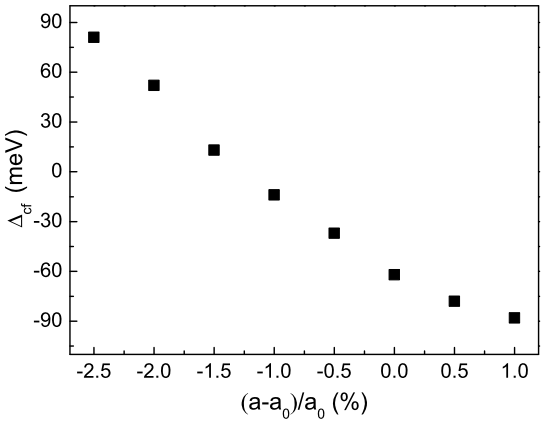

Fig. 4. The crystal field splitting energy as a function of in-plane biaxial strains.

coefficient $\alpha(\omega)$, refractive index $n(\omega)$, and energy-loss spectrum $L(\omega)$ can be derived from $\varepsilon_1(\omega)$ and $\varepsilon_2(\omega)$ [28].

Fig. 5 shows the real and imaginary part of the dielectric function of strained CZTS with the polarization perpendicular and parallel to the c-axis, compared with the unstrained CZTS using PBE and B3LYP functional, respectively. The dielectric functions calculated using B3LYP functional shows significant shift to higher energy with respect to the ones using PBE functional, which is consistent with the calculated bandgap. The imaginary part $\varepsilon_2(\omega)$ calculated by B3LYP functional displays a peak in the photon energy around 3 eV, which is in good agreement with the experimental report in the visible spectral range [29]. Meanwhile, it is also found that biaxial compressive strain pushes the high energy peaks to higher energy. This is because the electronic orbital hybridization, band splitting, and atom interaction are strongly affected by the strain, which results in the modification of electronic band structures. The results for the dispersive part of the dielectric function $\varepsilon_1(\omega)$ of the CZTS polycrystalline are also given in Fig. 5. The main features of the real part using B3LYP functional in our calculated unstrained CZTS are: (i) a peak located at around 2 eV and another two lower peaks located at about 4.7 and 7.4 eV; (ii) a rather steep decrease between 4.7 and 9 eV, inside of which $\varepsilon_1(\omega)$ decreases towards zero then becomes negative and finally reaches a minimum; and (iii) again a slow increase towards zero at higher energies. Strains have different effects on static dielectric constant, which could be estimated form the real part of the dielectric function ε_1 for $\omega \to 0$, dependent on the polarization direction. In the transverse ($\perp$, perpendicular to the c-axis) directions, static dielectric constant $\varepsilon^{\perp}$ increases with decreasing biaxial compressive strain and with increasing biaxial tensile strain whereas the opposite holds for $\varepsilon^{\parallel}$ (parallel to the c-axis). All the static dielectric constants are listed in Table 2.

Table 2
The static dielectric constant in the transverse and longitudinal directions.

	PBE			B3LYP		
ε_{11} (%)	−1.5	0	+1	−1.5	0	+1
	7.11	7.19	7.35	3.84	3.90	3.98
	6.72	6.55	6.49	3.78	3.67	3.64

Absorption coefficient is one of the most important parameters for absorber layer materials in their photovoltaic applications. The absorption coefficient, as shown in Fig. 6, obtained directly from the dielectric function [28], presents the linear optical response of kesterite CZTS from the VBs to the lowest CBs. The order of magnitude is about 10^4 cm^{-1} in the visible light region, which is in agreement with other reports [25,30]. The large value of the absorption coefficient is an advantage for the band-edge absorption

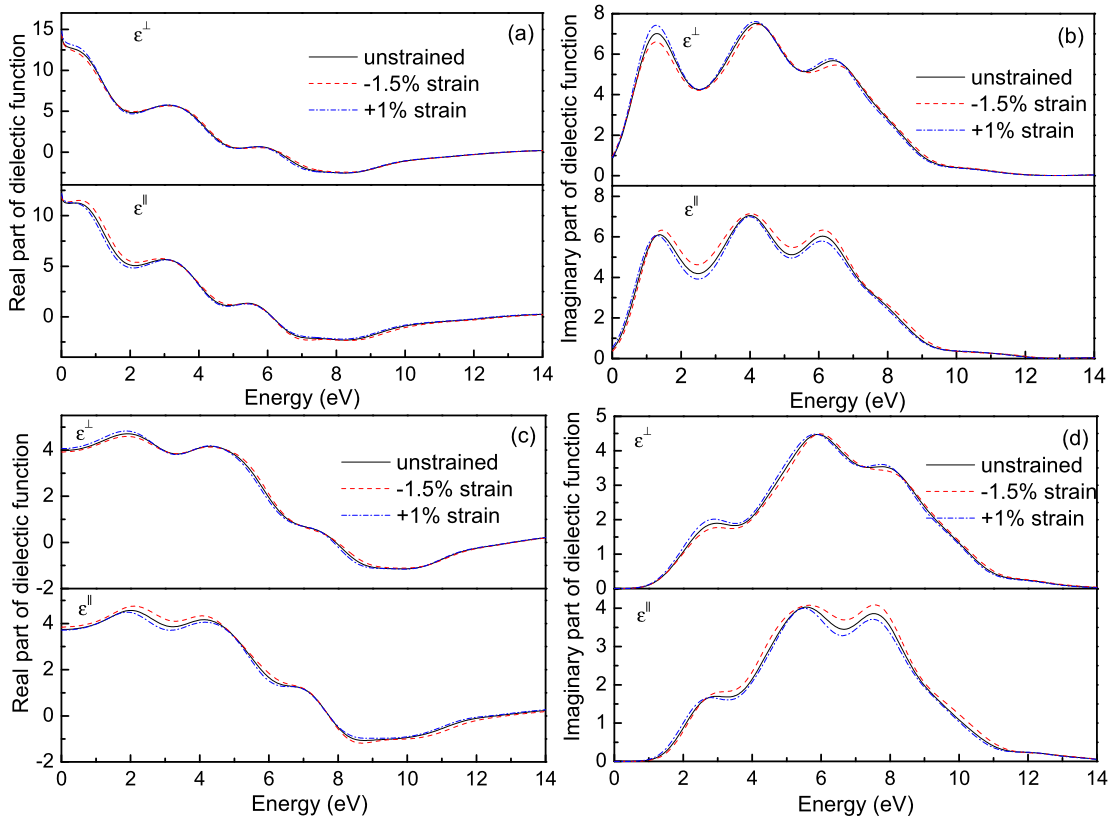

Fig. 5. Real and imaginary parts of dielectric function of the kesterite CZTS. (a), (b) are calculated with PBE functional and (c), (d) are calculated with B3LYP functional. Dash, dot and solid lines represent −1.5%, +1% biaxial strain and unstrained results, respectively.

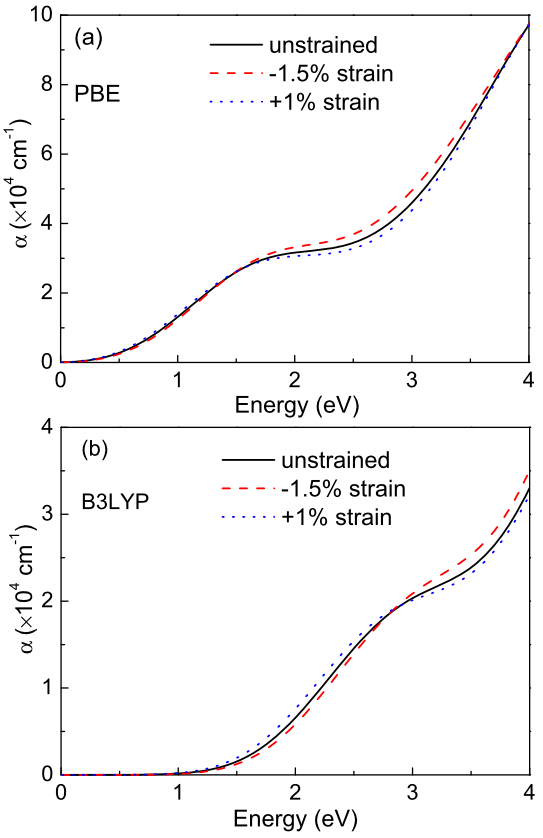

Fig. 6. Calculated absorption coefficient of the kesterite CZTS using (a) PBE and (b) B3LYP functional. Dash, dot and solid lines represent −1.5%, +1% biaxial strain and unstrained results, respectively.

efficiency in CZTS-based solar cells. It indicates that the value increases corresponding to increasing the strain from −1.5% to +1% at the photon energy of 2.5 eV. The phenomena could be attributed to the decrease of the electronic transition energy with the strain, which results in more photons being absorbed.

4. Summary

In conclusion, the electronic and optical properties of thin CZTS under various in-plane biaxial strains were investigated by first-principles calculations in details. The fundamental bandgap of CZTS does not monotonously change with biaxial strain. There exists a maximum as compressive biaxial strain is 1.5%. The change trend of optical bandgap is consistent with fundamental bandgap under biaxial strain.

Acknowledgements

This work was supported by the National Natural Science Foundation of China under grant Nos. 10874178, 11074093, 61205038 and 11274135, Natural Science Foundation of Jilin province under grant No. 201115013, National Found for Fostering Talents of Basic Science under grant No. J1103202, and the Ph.D. Programs Foundation of Ministry of Education of China under granted No. 20120061120011. This work was also supported by High Performance Computing Center of Jilin University, China.

References

[1] C. Steinhagen, M.G. Panthani, V. Akhavan, B. Goodfellow, B. Koo, B.A. Korgel, J. Am. Chem. Soc. 131 (2009) 12554.
[2] T.K. Todorov, K.B. Reuter, D.B. Mitzi, Adv. Mater. 22 (2010) E156.
[3] K. Wang, B. Shin, K.B. Reuter, T. Todorov, D.B. Mitzi, S. Guha, Appl. Phys. Lett. 98 (2011) 051912.
[4] C. Persson, J. Appl. Phys. 107 (2010) 053710.
[5] F.Y. Liu, Y. Li, K. Zhang, B. Wang, C. Yan, Y.Q. Lai, Z.A. Zhang, J. Li, Y.X. Liu, Sol. Energy Mater. Sol. Cells 94 (2010) 2431.
[6] K. Tanaka, N. Moritake, H. Uchiki, Sol. Energy Mater. Sol. Cells 91 (2007) 1199.
[7] T.K. Todorov, J. Tang, S. Bag, O. Gunawan, T. Gokmen, Y. Zhu, D.B. Mitzi, Adv. Energy Mater. 3 (2013) 34.
[8] W. Shockley, H.J. Queisser, J. Appl. Phys. 32 (1961) 510.
[9] J.M. Wagner, F. Bechstedt, Phys. Rev. B 66 (2002) 115202.
[10] Y.F. Li, B. Yao, Y.M. Lu, Y.Q. Gai, C.X. Cong, Z.Z. Zhang, D.X. Zhao, J.Y. Zhang, B.H. Li, D.Z. Shen, X.W. Fan, Z.K. Tang, J. Appl. Phys. 104 (2008) 083516.
[11] Y.F. Li, B. Yao, Y.M. Lu, C.X. Cong, Z.Z. Zhang, Y.Q. Gai, C.J. Zheng, B.H. Li, Z.P. Wei, D.Z. Shen, X.W. Fan, L. Xiao, S.C. Xu, Y. Liu, Appl. Phys. Lett. 91 (2007) 021915.
[12] Z. Alahmed, H. Fu, Phys. Rev. B 77 (2008) 045213.
[13] Y.Q. Gai, B. Yao, Y.M. Lu, D.Z. Shen, J.Y. Zhang, D.X. Zhao, X.W. Fan, Phys. Lett. A 372 (2007) 72.
[14] S. Chen, L.-W. Wang, A. Walsh, X.G. Gong, S.-H. Wei, Appl. Phys. Lett. 101 (2012) 223901.
[15] M.D. Segall, P.J.D. Lindan, M.J. Probert, C.J. Pickard, P.J. Hasnip, S.J. Clark, M.C. Payne, J. Phys.: Condens. Matter 14 (2002) 2717.
[16] D. Vanderbilt, Phys. Rev. B 41 (1990) 7892.
[17] A.D. Becke, J. Chem. Phys. 98 (1993) 5648.
[18] J. Muscat, A. Wander, N.M. Harrison, Chem. Phys. Lett. 342 (2001) 397.
[19] S. Schorr, H.-J. Hoebler, M. Tovar, Eur. J. Mineral. 19 (2007) 65.
[20] S. Chen, X.G. Gong, A. Walsh, S.-H. Wei, Phys. Rev. B 79 (2009) 165211.
[21] J. Paier, R. Asahi, A. Nagoya, G. Kresse, Phys. Rev. B 79 (2009) 115126.
[22] N.B.M. Amiri, A. Postnikov, Phys. Rev. B 82 (2010) 205204.
[23] B. Jogai, Phys. Rev. B 57 (1998) 2382.
[24] I. Camps, J. Coutinho, M. Mir, A.F.d. Cunha, M.J. Rayson, P.R. Briddon, Semicond. Sci. Technol. 27 (2012) 115001.
[25] H. Zhao, C. Persson, Thin Solid Films 519 (2011) 7508.
[26] H. Katagiri, N. Sasaguchi, S. Hando, S. Hoshino, J. Ohashi, T. Yokota, Sol. Energy Mater. Sol. Cells 49 (1997) 407.
[27] S. Chen, X.G. Gong, A. Walsh, S.-H. Wei, Appl. Phys. Lett. 94 (2009) 041903.
[28] J. Sun, H.-T. Wang, J. He, Y. Tian, Phys. Rev. B 71 (2005) 125132.
[29] W. Li, K. Jiang, J. Zhang, X. Chen, Z. Hu, S. Chen, L. Sun, J. Chu, Phys. Chem. Chem. Phys. 14 (2012) 9936.
[30] J.S. Seol, S.Y. Lee, J.C. Lee, H.D. Nam, K.H. Kim, Sol. Energy Mater. Sol. Cells 75 (2003) 155.